Quasi-periodical kinetic instabilities in minimum-B confined plasma

Cite as: AIP Advances **12**, 015223 (2022); https://doi.org/10.1063/5.0070824
Submitted: 09 September 2021 • Accepted: 05 January 2022 • Published Online: 24 January 2022

B. S. Bhaskar, H. Koivisto, O. Tarvainen, et al.

Quasi-periodical kinetic instabilities in minimum-B confined plasma

Cite as: AIP Advances 12, 015223 (2022); doi: 10.1063/5.0070824
Submitted: 9 September 2021 • Accepted: 5 January 2022 •
Published Online: 24 January 2022

B. S. Bhaskar,[1,2,a] H. Koivisto,[1] O. Tarvainen,[1,3] T. Thuillier,[2] and V. Toivanen[1]

AFFILIATIONS

[1] Department of Physics, University of Jyväskylä, P.O. Box 35 (YFL), 40500 Jyväskylä, Finland
[2] LPSC, INP Grenoble, CNRS/IN2P3, Université Grenoble-Alpes, 53 rue des Martyrs, 38026 Grenoble Cedex, France
[3] STFC ISIS Pulsed Spallation Neutron and Muon Facility, Rutherford Appleton Laboratory, Harwell OX11 0QX, United Kingdom

[a] **Author to whom correspondence should be addressed:** bisubhas@jyu.fi

ABSTRACT

We present the results of an experimental investigation of quasi-periodical kinetic instabilities exhibited by magnetically confined electron cyclotron resonance heated plasmas. The instabilities were detected by measuring plasma microwave emission, electron losses, and wall bremsstrahlung. The instabilities were found to be grouped into fast sequences of periodic plasma losses, separated by ~100 μs between the bursts, followed by 1–10 ms quiescent periods before the next event. Increasing the plasma energy content by adjusting the plasma heating parameters, in particular the magnetic field strength, makes the instabilities more chaotic in the time domain. Statistical analysis reveals that the energy released in a single instability event depends on the magnetic field strength and microwave power but not on the neutral gas pressure. The effects of these ion source parameters on the instability characteristics are explained qualitatively by considering their influence on the electron energy distribution. A correlation is found between the energy dissipated in an instability event and the recovery time of the periodic bursts, i.e., a large amplitude instability leads to a long recovery time of the electron energy distribution.

I. INTRODUCTION

Cyclotron maser instabilities caused by the resonant interaction between high energy electrons and electromagnetic waves are a fundamental feature of electron cyclotron resonance (ECR)-heated open plasma traps and minimum-B configurations with strongly anisotropic electron velocity distribution.[1,2] In the past, experimental studies of such instabilities have been conducted with magnetic mirror traps intended for thermonuclear fusion experiments[3] and simple mirror plasma generators dedicated for fundamental plasma physics studies.[4] In the pulse-periodic instability regime of the minimum-B confined plasma, the plasma–electromagnetic wave interaction results in abrupt bursts of microwave emission[5,6] and electrons escaping the confinement,[7] which in turn results in strong spikes of (thick target) bremsstrahlung emission (x ray) from the plasma chamber walls.[8] The instability-induced electron losses result in fast fluctuations of the plasma potential and subsequent ion losses including the extracted ion beam current,[9] significantly decreasing the average charge state of the ions both in the plasma and in the time-averaged extracted beam.[10,11]

Systematic studies of the cyclotron maser instabilities, fundamentals of which are described in Ref. 12, in the continuous operation mode of the ECRIS have revealed several stability regimes. The transition between them can be controlled by adjusting the source parameters,[8] most notably the magnetic field strength at the minimum-B (B_{min}), which is known to influence the electron energy distribution (EED)[7,13] and the x-ray emission of minimum-B ECRISs.[14,15] These regimes can be broadly categorized as (i) stable plasma with no detectable microwave emission above the background electron cyclotron emission (ECE), (ii) pulse-periodic regime with abrupt bursts of microwave emission at specific frequencies[5,16] and electron precipitation,[7] both observed at the 0.1–1 kHz order of the magnitude repetition rate,[8,17] (iii) pulsed regime characterized by very strong instabilities (referred to as "giant pulses" by some authors[5]) occurring at irregular intervals and corresponding to a rich frequency spectrum of the microwave emission,[6] and (iv) continuous maser emission regime.[18,19]

All cyclotron maser instabilities observed in the various regimes of ECRIS plasmas are caused by the temporal modulation of the

electron distribution function due to the excitation of unstable kinetic modes.[1] This is because distributions of fast electrons formed under electron cyclotron heating are usually unstable with respect to the excitation of electromagnetic waves in the same frequency range, as described thoroughly elsewhere.[20,21] Different dynamic regimes of the cyclotron maser instability represent different sets of steady-state solutions for the electron energy distribution $\left(\frac{\partial \tilde{f}}{\partial t}\right)$ and energy content $\left(\frac{\partial W}{\partial t}\right)$ balance equations. The solutions described in Ref. 20 include a continuous wave (cw) maser emission corresponding to a certain electromagnetic mode, i.e., regime (iv) mentioned above, as well as temporally modulated maser emission consisting of intense bursts of electromagnetic radiation (and subsequent electron precipitation) separated by long periods of small amplitude emission, i.e., regimes (ii) and (iii). The stable regime can be expanded notably in terms of magnetic field strength and microwave power by applying two-frequency heating.[22]

In the pulse-periodic solutions, the energy content of the EED oscillates between a minimum value following each instability burst and a maximum corresponding to the trigger level of the instability, at which the growth rate (γ) of the amplified electromagnetic (EM)-wave exceeds its damping rate (δ), i.e., $\frac{dE_\mu}{dt} \approx \langle \gamma - \delta \rangle E_\mu > 0$. The (volumetric) growth rate is proportional to the ratio of hot and cold electron densities, whereas the damping rate is determined by volumetric absorption of the wave energy by the background plasma and external (wall) losses (the reader is referred to the literature for the parametric dependencies of the growth and damping rates[23–25]). Between these extremes, the energy content of the EED builds up at a rate, which depends on the source (electron heating), $S(t)$, and loss, $L(t)$, and terms of hot electrons (rf-scattering, collisional losses, and energy damping by inelastic processes). The balance equation[20,26] for the hot electron (number) density $N_{e,hot}$ can be written as $\frac{dN_{e,hot}}{dt} \approx -\kappa N_{e,hot} E_\mu + S(t) - L(t)$, where κ is a coefficient[27] describing the amplification of the electromagnetic wave and the corresponding decrease of the hot electron number density due to direct energy loss. Thus, it can be hypothesized that the repetition rate of the instabilities is correlated with the source and loss terms during the quiescent period between instabilities, which are affected by the source parameters,[8,28] and with the energy loss associated with the instability. The latter implies that the energy accumulation time to reach the instability threshold should depend on the energy loss associated with the preceding instability event. In this scenario (a), the time between instability bursts depends on their magnitude, a large amplitude burst leading to long recovery time until the next event. Alternatively, the plasma parameters may be perturbed by the instability in such a manner that the threshold plasma energy content to trigger the instability shifts between consecutive bursts. In this scenario (b), a long accumulation time is followed by a large magnitude burst, releasing the energy stored in the hot tail of the EED.

Since both scenarios (a) and (b) are feasible and studies of magnetospheric plasmas have revealed that dynamics of the instabilities could depend on the magnitude of the energy dissipation in an instability event,[29] we have carried out an experimental campaign measuring the correlation between the instability signal amplitudes and the recovery/accumulation times (see the definitions below) in a controlled laboratory experiment with a minimum-B ECRIS. In particular, we focus on parametric dependencies of the energy dissipation by the instability and the dependence of recovery and accumulation times of the dissipated energy. This is done to demonstrate that one of the above scenarios appears to be a fundamental feature of the minimum-B trap, independent of control parameters (magnetic field strength, microwave power, and neutral gas pressure). By recovery time, we refer to the time following an instability event required to restore the unstable EED, whereas by accumulation time, we refer to the time preceding the instability event, i.e., the recovery time of instability event i is the accumulation time of event $i+1$. One can also define the period of the instability event i as the sum of the event time i (time during which one or several bursts are observed) and the recovery time i. The main purpose of this experimental study is to support the development of the practical cyclotron maser theory[21] applicable for ECR-heated laboratory plasmas serving as a proxy for a range of naturally occurring plasmas where such phenomena can exist.[24,30–32] This is achieved by carrying out a phenomenological investigation of the instability energy dissipation and recovery/accumulation times as a function of ECRIS tuning parameters, namely, the strength of the solenoid magnetic field, microwave heating power, and neutral gas density. Based on previous studies, these parameters are believed to affect the plasma parameters as follows: the magnetic field strength affects the electron energy distribution and average energy, while the microwave power and neutral gas density affect the plasma density (for detailed discussion, see, e.g., Ref. 15 and references therein).

II. EXPERIMENTAL SETUP AND PROCEDURE

The experimental data were taken with the A-ECR type JYFL 14 GHz ECR ion source[33] at the Accelerator Laboratory of the University of Jyväskylä. The source is a room-temperature ECRIS operated at the 14.055 GHz plasma heating frequency. The minimum-B magnetic field structure for plasma confinement is produced with two solenoid coils (axial mirror fields) and a NdFeB permanent magnet hexapole (radial mirror field). The nominal on-axis magnetic field maxima are 1.93 T in the injection side of the plasma chamber (B_{inj}) and 0.90 T in the extraction side (B_{ext}). The nominal minimum field (B_{min}) inside the chamber is 0.35 T and the radial maximum at the chamber wall is B_{rad} = 1.09 T when the solenoids are not energized. The axial magnetic field can be varied by adjusting the solenoid currents, which also affects the strength of the radial field in those locations where the plasma flux meets the chamber wall.

In our experiment, the plasma density in the core plasma can be expected to range from 10^{11} to 2.5×10^{12} cm^{-3}, where the lower limit has been defined experimentally on a similar device[34] and the upper limit corresponds to the cutoff frequency of 14 GHz microwaves. The spatial variation of the plasma density can be expected to be very strong, with the core plasma surrounded by the closed ECR zone reaching the aforementioned densities,[35,36] whereas the peripheral plasma density is 1–2 orders of magnitude lower. It has been estimated that each instability onset expels ~0.1–1 μC of negative charge, with the upper limit corresponding to ~10% of the confined electron population.[9] ECRIS plasmas are strongly anisotropic and are considered to consist of cold electrons (created by ionizing electron–ion collisions and plasma–wall interaction) with an average energy $E_{\mathrm{e,cold}}$ of 10–100 eV, warm electrons responsible for the stepwise ionization with an $E_{\mathrm{e,warm}}$ of 1–10 keV, and hot electrons with an $E_{\mathrm{e,hot}}$ of 10–100 keV.[37,38] It has been shown previously[13]

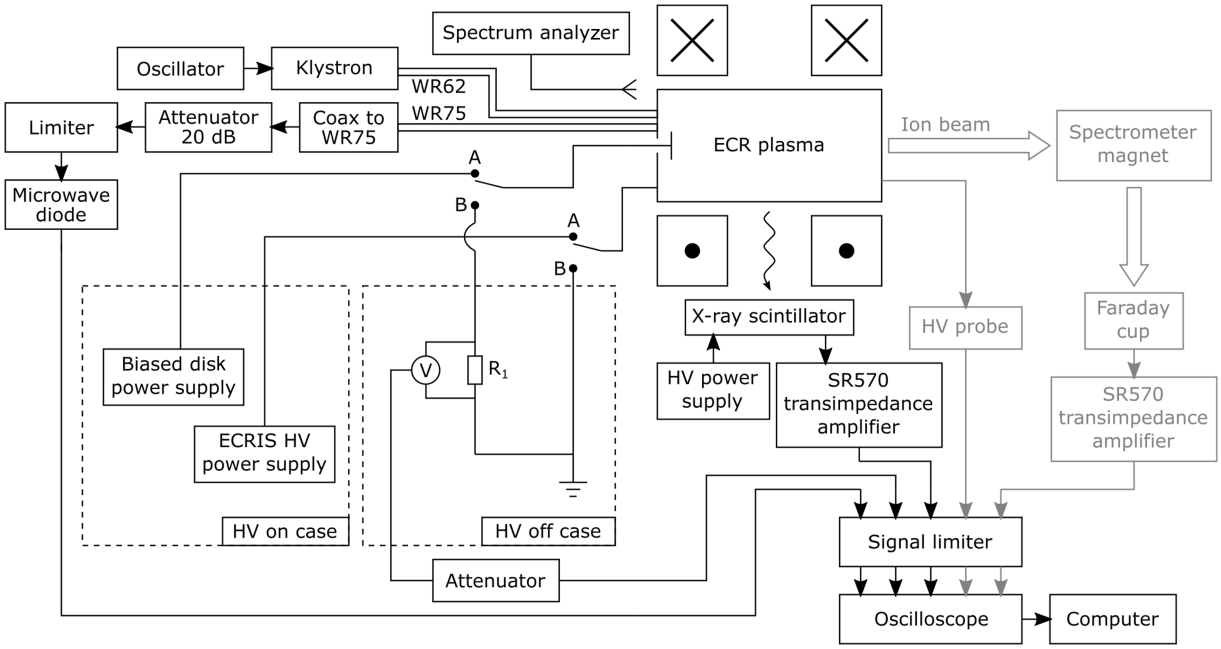

FIG. 1. A schematic presentation of the experimental setup. For simplicity, the different connections for the two measurement modes, high voltage (HV) on and HV off, have been presented with two switches, both of which are simultaneously toggled either to the *A* (HV on) or *B* (HV off) position. In order to ensure that the ion source was functioning properly during the experiments, the extracted ion beam currents and the source HV platform voltage were also monitored. These signals are not part of the reported instability analysis but are presented in the schematic (in gray) for the sake of completeness.

that in our setup, the EED (of axially escaping electrons) is strongly non-Maxwellian with a maximum electron energy of ~500 keV.

Figure 1 presents the experimental setup and the different diagnostics used in the measurements. Two waveguides can be used to transmit microwaves into the plasma chamber. The main (WR62) waveguide was used for plasma heating, connecting the plasma chamber to a klystron amplifier driven by an oscillator providing the 14.055 GHz heating frequency. The secondary (WR75) waveguide was used for microwave diagnostics. The microwave emission from the plasma was measured with a microwave-sensitive Schottky diode. A WR75-to-coax adapter was used to connect the diode to the waveguide. In addition, a 20 dB (20 W) attenuator and a microwave signal limiter were placed in the coaxial line between the ion source and the diode to protect it from the potentially very strong signals that can occur during the instability events. The microwave emission was also detected with a spectrum analyzer (Keysight FieldFox Microwave Analyzer N9918B). This was done because distributions of fast electrons formed under strong electron cyclotron heating are usually unstable with respect to excitation of electromagnetic waves in the same frequency range.[21] Thus, we use the microwave emission spectrum to confirm that the above condition for maser-type kinetic instabilities is met in our experiment. An example of the emission spectrum recorded with 7.8 s sweep time across the presented frequency range is shown in Fig. 2. It is emphasized that the spectrum analyzer cannot measure individual bursts but rather the overall emission spectrum consisting of frequencies emitted in multiple instability onsets, as thoroughly explained elsewhere.[39] The data are presented to make the point that the microwave radiation frequencies emitted by the instabilities are characteristic to our experimental setup and are predominantly lower than the plasma heating frequency (with their harmonics found above 20 GHz).[5,6]

The 21 mm diameter circular biased disk located at the injection end of the plasma chamber was used to probe the electron

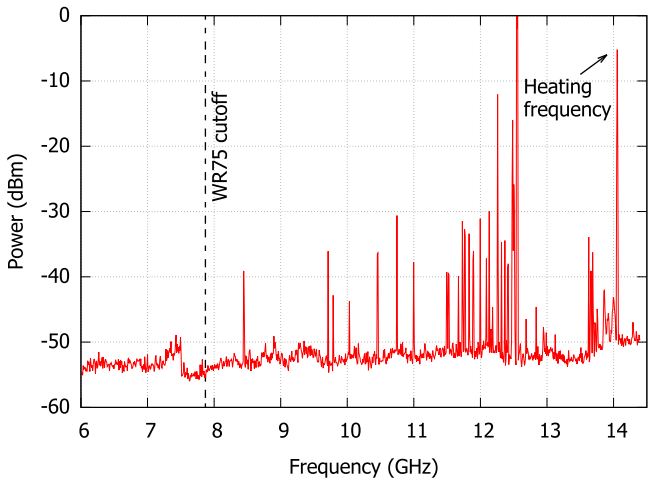

FIG. 2. Microwave emission spectrum measured with a spectrum analyzer during unstable plasma conditions. The emission frequencies are discrete. The emission peak corresponding to the plasma heating frequency (14.055 GHz) is indicated with an arrow. The WR75 waveguide cutoff frequency (7.87 GHz) is also indicated with a vertical dashed line. In the stable regime, the only detectable emission is at the heating frequency.

and ion losses during the instabilities. As demonstrated earlier,[9] the electron and ion signals recorded with the biased disk provide quantitative information on the negative and positive charge expelled from the plasma through the injection end mirror at each instability burst.

The bursts of thick target x-ray emission from the plasma chamber walls, caused by the electron losses during the instability events, were recorded with a bismuth germanate (BGO) scintillator coupled with a Na-doped CsI photocathode and a photo-multiplier tube (PMT). The detector was operating in the DC (or current) mode, allowing the detection of both the instability-induced x-ray bursts and the continuous background signal. The scintillator was placed outside the ion source plasma chamber and the hexapole. Axially the scintillator was located at the center of the plasma chamber between the iron yokes of the solenoid coils and azimuthally at one of the poles of the hexapole magnet structure. A −700 V bias was supplied to the PMT from a separate power supply. The bias voltage sets the gain and detection threshold of the PMT and, thus, the bias voltage was kept constant throughout the experimental campaign. The PMT output was amplified and converted to a voltage signal with a transimpedance amplifier (Stanford Research Systems SR570).[40] In such a configuration, the detector signal is proportional to the x-ray power flux but cannot be used for quantitative measurements of electron losses as the efficiency of the scintillator depends on the photon energy and the photon energy spectrum depends on the EED causing x-ray emission from the wall.

All the diagnostic signals were recorded with a picoscope (model 5444B).[41] The signals were routed through a diode based signal level limiter with a ±25 V limiting threshold to protect the picoscope from input signal overload, which could potentially occur in the pulsed instability regime with the strongest instability events, i.e., regime (iii) mentioned previously.

The microwave power, magnetic field, and gas feed were varied to produce a range of unstable plasma conditions within regimes (ii) and (iii). Each of these parameters was varied independently, while the others were kept constant during the parameter sweeps: The microwave power was varied between 400 and 600 W, while keeping both coil currents at 540 A ($B_{\mathrm{min}}/B_{\mathrm{ECR}} = 0.774$) and the plasma-off gas pressure at $3.5 \cdot 10^{-7}$ mbar, recorded with an ionization gauge connected to one of the radial ports of the plasma chamber. The coils were varied between 535 and 575 A ($B_{\mathrm{min}}/B_{\mathrm{ECR}}$ between 0.765 and 0.837) with 400 W microwave power and $3.5 \cdot 10^{-7}$ mbar pressure. The chamber pressure was varied between $3.0 \cdot 10^{-7}$ and $4.5 \cdot 10^{-7}$ mbar (plasma off values) with 300 W microwave power and 575 A coil currents ($B_{\mathrm{min}}/B_{\mathrm{ECR}} = 0.837$). In order to confirm the reproducibility of the data, the data acquisition for the magnetic field sweep was conducted twice. The reproducibility of the data is discussed and illustrated in the supplementary material (Fig. S6), showing a very good agreement between the two datasets (with a relative discrepancy ≤3.5%), which strengthens the conclusions of the study. All measurements were performed with oxygen plasmas as the majority of the published experiments (see Refs. 1, 5, 8–10, 22, and 42–49) investigating the instabilities in our setup have been conducted with oxygen. The characteristics of the instabilities are found to be similar with other gases, e.g., helium, argon, or xenon, whereas the gas affects the exact magnetic field threshold of the transition between stable and unstable regimes,[11] presumably due to different inelastic collision rates affecting the instability damping rate.

In order to allow simultaneous recording of the biased disk signal with the other diagnostics using the same measurement earthing, the experiments were performed both with and without the ion source high voltage. In the measurements with the high voltage, the source potential was set to 10 kV and the biased disk was connected to a −1 kV/10 mA power supply set to −70 V (a typical value for operation). The biased disk power supply was floating on the source potential. In this configuration, the microwave and x-ray signals were recorded concurrently. For the instability-induced biased disk electron/ion flux measurements, the plasma chamber was earthed and the disk power supply was disconnected. The current of the biased disk was monitored by measuring the voltage across a 1 kΩ series resistor, which was added between the disk and the laboratory earthing. A 12 dB attenuator was used to reduce the biased disk signal during the instabilities to a suitable level for the data acquisition. In this configuration, the microwave, biased disk, and x-ray signals were recorded simultaneously.

The operation with the high voltage on is the *modus operandi* of the ECR ion source, and it has been shown that applying the source potential affects the plasma parameters[50,51] and the instability threshold.[8] On the other hand, the x-ray signal is affected by the escaping electron energy distribution, attenuation of the photon flux in the structure of the ion source, and location of the scintillator and its efficiency, whereas the microwave emission signal strength depends on the coupling of the microwave radiation to the (diagnostics) waveguide and its attenuation in the waveguide, i.e., the amplitude of the detected signal is strongly affected by the frequency of the emitted microwaves. Hence, the instability-induced biased disk current transient (recorded with HV off) can be considered to be the most primitive diagnostics, directly measuring the

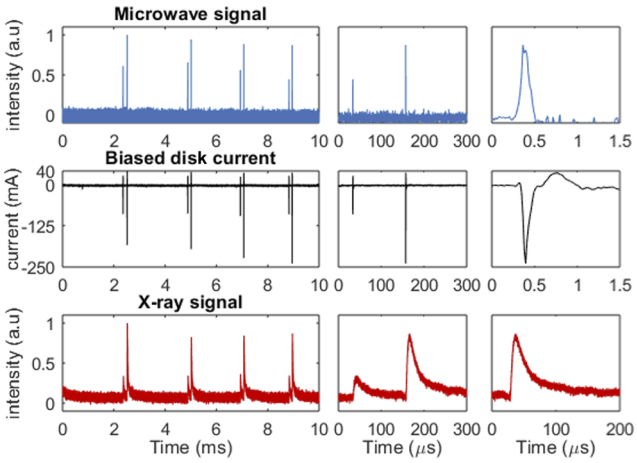

FIG. 3. An example of simultaneous detection of instability-induced signals with different diagnostic methods. Here, the instability events are separated by ∼2 ms and consist of two bursts (referred to as mode $n = 2$ later). The two stage zoom on the right illustrates the characteristic time scale between the bursts within an instability event, separated by ∼100 μs, and that of a single burst. The microwave and electron bursts of the biased disk (negative signal) last ∼0.2 μs, the latter being followed by a burst of ions (positive signal), restoring the quasi-neutrality of the plasma. The decay time of the x-ray signal is defined by the RC-constant of the transimpedance amplifier.

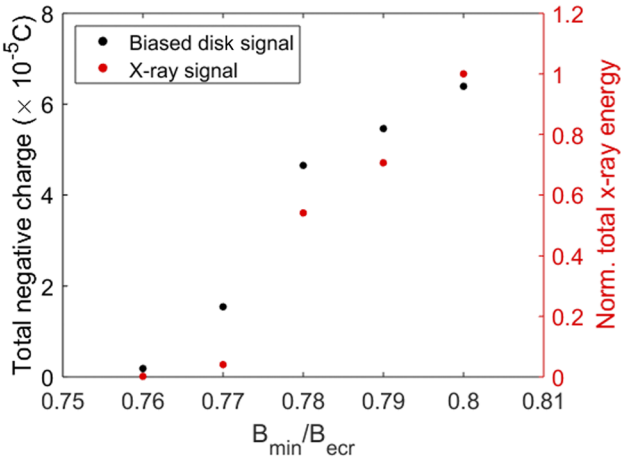

FIG. 4. The effect of the *B*-field on the total negative charge expelled by the instabilities measured from the biased disk and the measured total x-ray energy. The observables are integrated, i.e., individual burst signals are summed, over the 10 s data acquisition time at each magnetic field setting. The methodology to calculate the normalized plasma energy loss from the measured x-ray signal is described in the supplementary material. The pressure was kept constant at 3.5×10^{-7} mbar and the RF power at 600 W.

charge (negative and positive) expelled by each burst to the ion source injection end. Figure 3 shows an example of the diagnostic signals exhibiting abrupt bursts characteristic to the pulse-periodic maser instability. For each ion source setting, a total of 10 s of data were recorded to accumulate a sufficient amount of statistics. The data were recorded in 1 s segments with a temporal resolution of 16 ns used for all diagnostic signals.

In Secs. III and IV, we will use the x-ray signal for the majority of the data analysis and presentation. This is because under certain ion source parameters and instability sequences, no microwave emission bursts corresponding to instability-induced x-ray bursts were registered. Due to the physical nature of the instabilities, microwave emission can always be expected to correlate with the x-ray signal, and thus, the "missing" microwave bursts are associated with the emission at (low) frequencies[6] being suppressed or cut off by the diagnostic waveguide (an example is shown in Fig. S5 of the supplementary material). On the other hand, the energy dissipated via x-ray emission correlates well with the total electron charge Q expelled from the plasma by the instabilities and recorded from the biased disk ($Q = \int I_{BD} dt$, where I is negative), with an example from the magnetic field sweep shown in Fig. 4. This serves as a further justification to treat the x-ray signal as a more reliable diagnostic (over microwave emission) with the high voltage on.

III. DATA ANALYSIS

A. Peak detection and classification of periodic instability regimes

The data analysis was divided in two parts. Before the statistical analysis of correlation between accumulation/recovery times and instability signal amplitudes, it was necessary to classify different periodic instability regimes. In order to process the data, an inbuilt MATLAB peak detection function was used, which returns the timestamp (T) and full-width half-maximum (FWHM) corresponding to each peak of the recorded signals. For each ion source fixed set of parameters, ten measured cases of 1 s segments of data were merged together to form one 10 s dataset, after taking care of cleaning the incomplete first and last events of each 1 s data file.

The peak identification revealed the existence of several "modes" in the pulse-periodic instability regime. These are characterized by instability *events* at longer intervals, which can include a train of *bursts* at shorter time scales, i.e., a group of individual signal peaks within the event. These "modes" are defined here based on the number of individual bursts within the instability event with mode index n so that, for example, an instability event that includes three distinct separate bursts in quick succession is classified as $n = 3$. Figure 5 shows representative examples of different instability modes ($n = 1$, 2, 3, and 5) with single, double, triple and quintuple bursts in each event of instabilities. Furthermore, an index number m is defined here to indicate each separate burst within an event starting from the first one observed, so for each event of mode n, the index m runs from $m = 1, \ldots, n$. It is emphasized that these instability events, which for the given ion source settings are separated by milliseconds between them and in the order of 10–100 μs between each burst within the event, are different from the sequential instabilities occurring in μs time scale, exhibiting a falling tone of the emission microwave frequency, which have been reported in Ref. 5. The grouping of instability events to the "n-modes" discussed here resembles the patterns for a high-power gasdynamic mirror trap.[20]

The signal peak height (amplitude) of each burst was calculated from a baseline determined by the average background signal strength preceding an instability event, as illustrated in Fig. S1 of the supplementary material. It was then established with a dataset consisting of isolated ($n = 1$ mode) instability events that there is a linear correlation between the x-ray signal amplitude and area, as shown in Fig. S2 of the supplementary material. The integrated area of the x-ray peak, which is proportional to the plasma energy loss per

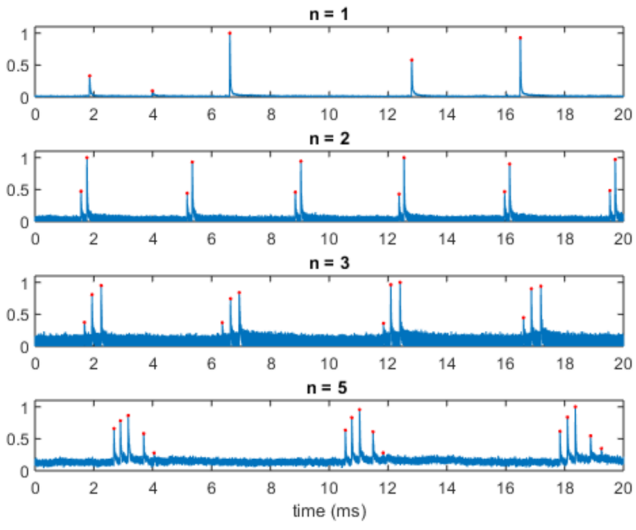

FIG. 5. An example of x-ray signals observed in different modes $n = 1$, 2, 3, and 5.

burst, was then calculated from this linear fit, allowing the code to automatically tabulate the timing, amplitude, and area of each peak.

B. Analysis of accumulation and recovery times

The occurrence of such "grouped" instabilities in event modes $n = 1, \ldots, 10$ complicates the analysis of the recovery and accumulation times as the instabilities do not appear at well-defined repetition rate but instead the time between individual instability bursts and events varies by an order of magnitude. Thus, the next step of the data analysis algorithm was set up to classify each burst (m) of each event (n). This was achieved by choosing an appropriate time threshold and comparing the time difference between a burst and its neighbors in both forward and backward directions in time, up to ten diagnostic signal peaks. The choice is based on the maximum number of bursts observed in a single grouped instability event. The time threshold was chosen by plotting the recovery time of instabilities for every burst, which typically results in two well-separated maxima of the distribution corresponding to different events n and bursts m (see Fig. S3 in the supplementary material for an example). The indexing of each peak with (n, m) allows studying the instability amplitudes and recovery/accumulation times between the events, i.e., as a function of n, as well as within each group, i.e., as a function of m. An example illustrating the n and m indexing of an event/bursts, as well as the definition of the accumulation and recovery times referring to events, is presented in Fig. 6.

IV. EXPERIMENTAL RESULTS AND DISCUSSION

A. Occurrence of instability events n and instability strength as a function of the ion source parameters

As a first step to interpret the data, we studied the prevalence of each instability event (n) as a function of the three main parameters of the ECRIS, i.e., magnetic field, microwave power, and neutral gas pressure. Figure 7 shows the fraction of each instability event mode n (out of all events) and the average of n for each setting. For

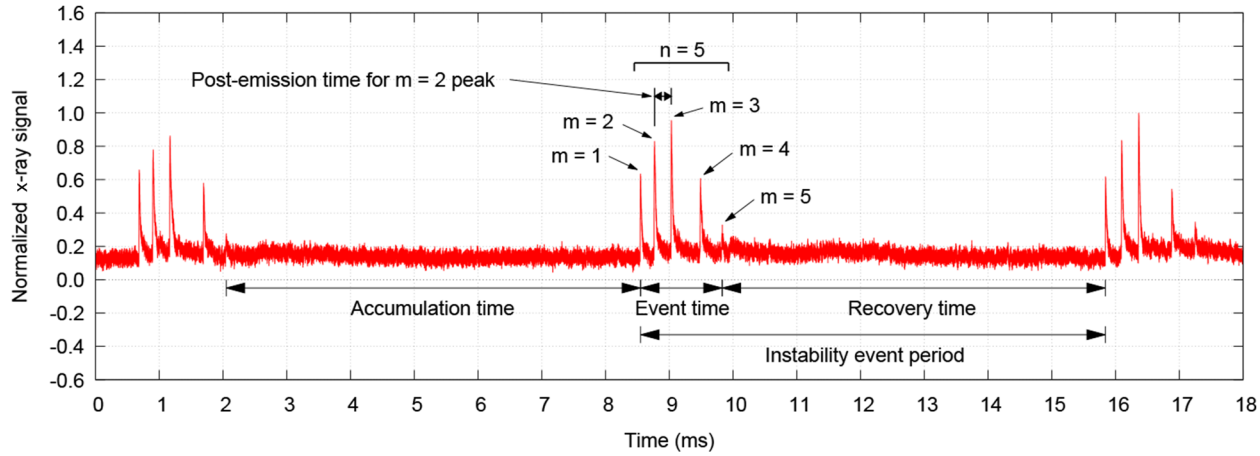

FIG. 6. An example of the determination of the burst numbers m, event (mode) number n and the accumulation time, event time, recovery time, and instability event period. The *instability event* is defined to be the group of bursts with $m = 1, \ldots, 5$, i.e., $n = 5$ in the example. The time from one burst to the next one within an event is denoted as *post-emission time*, presented here as an example for the $m = 2$ burst.

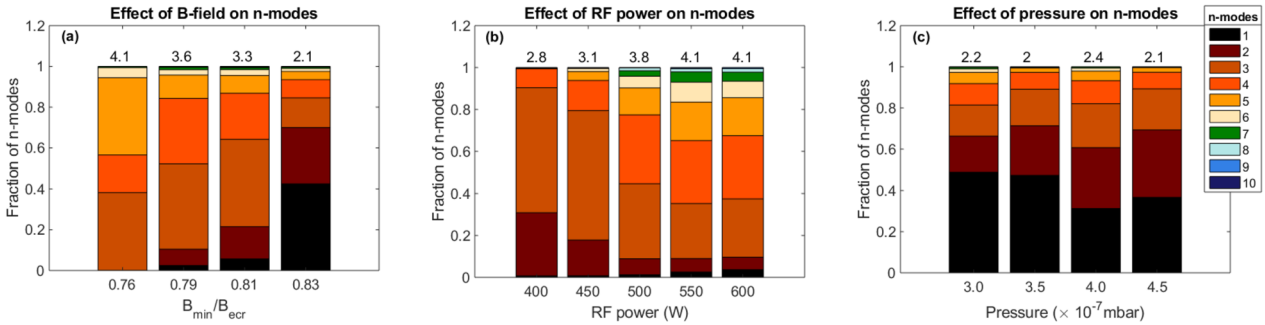

FIG. 7. The relative fraction of instability event mode n as a function of the ion source parameters. The average value of n is shown on top of each bar. In (a), B_{min}/B_{ecr} was increased keeping the neutral gas pressure and RF power constant at 3.5×10^{-7} mbar and 400 W, respectively. In (b), the RF power was increased keeping the B_{min}/B_{ecr} and neutral gas pressure constant at 0.78 and 3.5×10^{-7} mbar, respectively. In (c), the neutral gas pressure was increased keeping the B_{min}/B_{ecr} and RF power constant at 0.83 and 300 W, respectively.

the magnetic field sweep, the results are shown as a function of the B_{min}/B_{ECR} ratio, which has been found to be a good measure of the instability threshold[8] and energy content of the EED.[13]

It is seen that at low field strength, there are no isolated (n = 1) instabilities, but they become the prevalent event mode at the strongest field setting. Overall, the number of observable modes (different n) increases and the average number of bursts per instability event (average n) decreases with increasing magnetic field strength. At the same time, the total energy (power) dissipated via instabilities increases with the magnetic field strength, as seen in Fig. 8 showing the integrated area of the x-ray signals, which is proportional to total energy dissipation by the expelled electrons, as a function of the source parameters. With increasing microwave power, the number of existing modes (n) and the average number of bursts per instability event were observed to increase. At the same time, the total energy dissipated via the instabilities increases linearly with the power.

The total dissipated energy increases with the magnetic field and microwave power, as shown in Fig. 8. This can be explained with these parameters affecting the electron heating rate, i.e., the decrease of the magnetic field gradient at the resonance and the increase of the direct power input to the plasma volume. Consequently, the threshold plasma energy content to trigger the plasma instability is reached faster, which is seen as the decrease of the instability event period and thus, the total energy expelled by the instabilities in a given time increases. It is also seen in Fig. 8 that the magnetic field has a stronger impact on the total emitted energy when compared to the effect of the microwave power. This is explained by the greater influence of the magnetic field on the high energy tail of the EED compared to the effect of the microwave power observed either indirectly through bremsstrahlung spectrum[14,15] or directly through the measurement of the energy distribution of electrons escaping from the minimum-B confinement.[7,15] Furthermore, it has been shown that in the ECRIS plasmas, the magnetic field strength, especially the value at the center of the trap (B_{min}), affects the threshold between the transition from the stable to the unstable regime[8] and further into the continuous maser emission regime[18] more than the applied microwave heating power or neutral gas density. It is worth noting that the relation between the heating regime (including the magnetic field) and the related instability dynamics was first considered by Demekhov and Trakhtengerts.[52] The present data provide further input for theoretical considerations.

The neutral gas pressure has an insignificant effect on the distribution of the event modes n. In the case of the neutral gas sweep, the prevailing mode was n = 1, whereas the number of n-modes was observed to increase with decreasing neutral gas pressure with n up to nine, detected with the lowest pressure. The prevalence of n = 1 is most likely due to the magnetic field strength (B_{min}/B_{ECR} = 0.83) being more important in determining the instability dynamics than the neutral gas pressure. The total energy dissipated by the instabilities was observed to be almost constant across the range of the neutral gas pressure sweep despite the plasma density being higher for high gas pressure (indicated by the concomitant increase of the total extracted current). This implies that the strength of the instability is independent of the plasma density but rather depends on the electron heating affected by the B-field[15,53,54] and microwave power.[55]

The parametric dependencies can be explained by the effect of the magnetic field, microwave power, and neutral gas pressure on the EED. When B_{min} is increased, the hot (>100 keV part) tail of the EED is affected, which causes the instability induced bremsstrahlung power emission to increase drastically. The change in the microwave power has a weaker effect on the burst of bremsstrahlung power associated with the instabilities as it does not affect the shape of the EED but the electron density and electron flux instead. The change in the neutral gas pressure has an insignificant effect on the (hot) electron population, relevant for the instabilities, which explains the insensitivity to this parameter. All these parametric effects on the EED have been confirmed experimentally by measuring the EED of the electron flux escaping the confinement axially through the extraction aperture.[13,15] It is worth noting that the EED of the escaping electron flux could be different from the EED of the confined electrons. The effect of each parameter (B-field, microwave power, and neutral gas pressure) on the instabilities strengthens the argument that the parametric dependencies of the EED of escaping and confined electrons are similar. In summary, the parametric sweeps presented here revealed that the distribution of the instability modes n is affected most by the magnetic field strength, followed by the microwave power, and least affected by the neutral gas pressure.

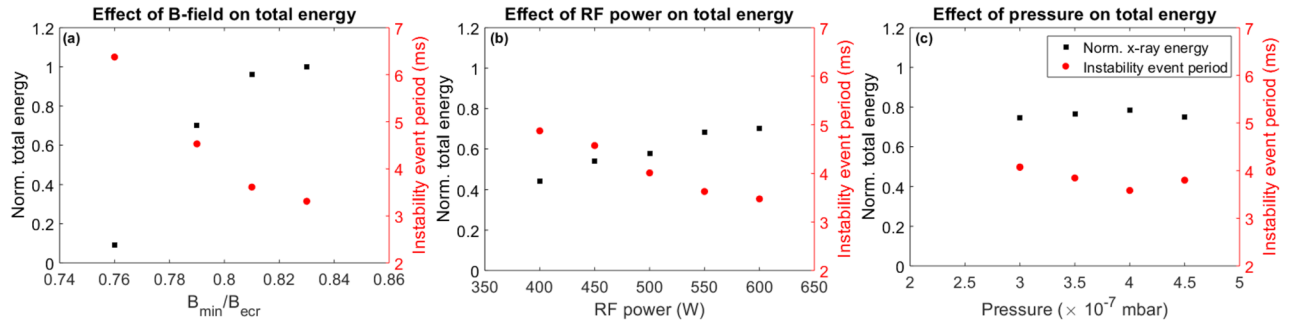

FIG. 8. The total dissipated energy (relative) as a function of the ion source parameters. In (a), B_{min}/B_{ecr} was increased keeping the neutral gas pressure and RF power constant at 3.5×10^{-7} mbar and 400 W, respectively. In (b), the RF power was increased keeping the B_{min}/B_{ecr} and neutral gas pressure constant at 0.78 and 3.5×10^{-7} mbar, respectively. In (c), the neutral gas pressure was increased keeping the B_{min}/B_{ecr} and RF power constant at 0.83 and 300 W, respectively. The normalization is performed with respect to the largest value corresponding to all three sweeps. The second y axis represents the event period (see Fig. 6 for definition).

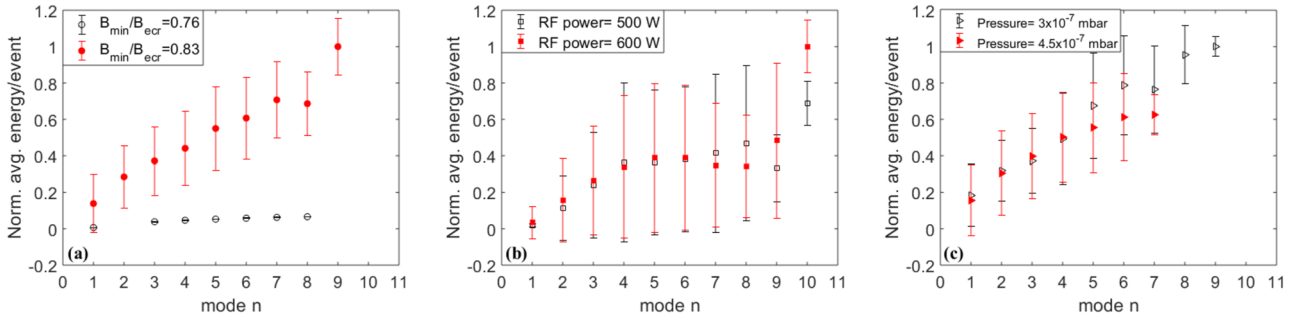

FIG. 9. The dependence of energy emitted per instability event vs n for selected examples of ion source parameters: (a) the magnetic field strength, (b) the microwave power, and (c) the neutral gas pressure. The plots are normalized to the maximum average energy/mode among all three cases.

B. Energy dissipation and characteristic times as a function of the instability event mode n

Next, we studied the average energy dissipated in an instability event as a function of n. It was observed that the energy tends to increase with n. This is shown in Fig. 9, displaying the average integrated area of x-ray emission peaks per event (normalized) as a function of n for two B-field, power, and pressure values, chosen as representative examples. The integration is carried out over all bursts m in each event n. The error bars correspond to the standard deviation of the total energy histograms, specifically selecting

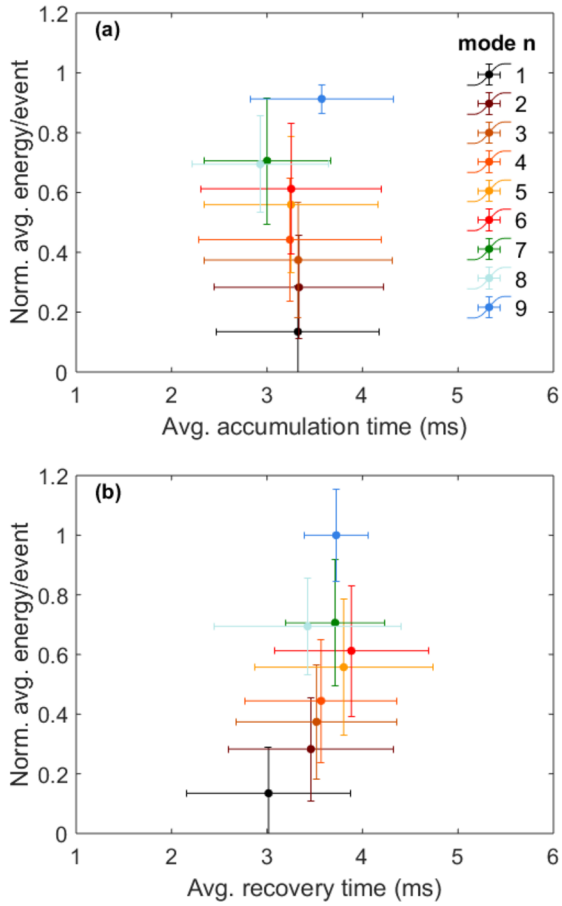

FIG. 10. The average energy emitted per event vs the accumulation (a) and recovery times (b) for a B_{min}/B_{ecr} value of 0.83, neutral gas pressure of 3.5×10^{-7} mbar, and RF power of 400 W.

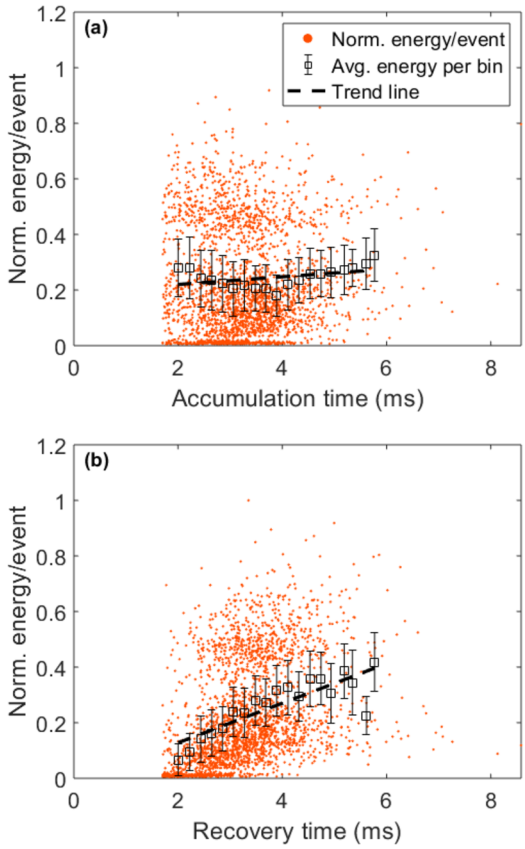

FIG. 11. The accumulation (a) and recovery times (b) as a function of the energy emitted per event. The temporal axis is divided into 20 bins, and the average energy per event and its standard deviation is calculated for each bin. The plot corresponds to a B_{min}/B_{ecr} of 0.83, 3.5×10^{-7} mbar neutral gas pressure, and 400 W RF power.

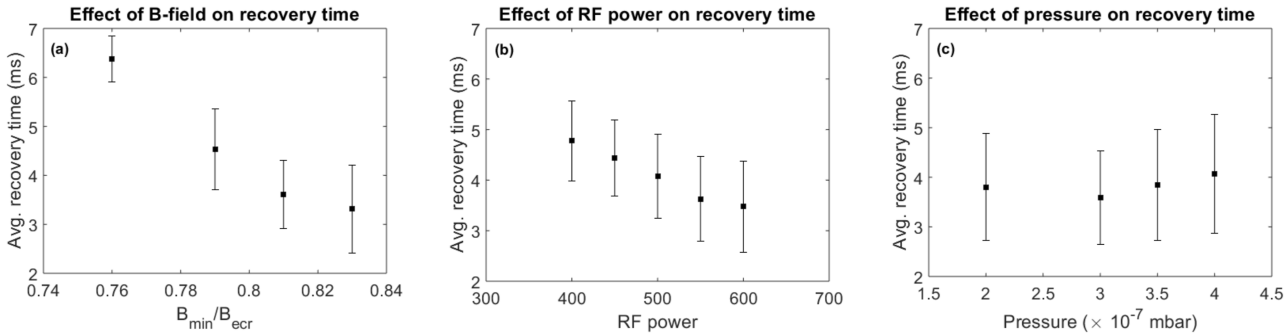

FIG. 12. The dependence of instability recovery time on (a) B_{min}/B_{ecr}, (b) RF power, and (c) neutral gas pressure.

instability events with a certain n. The energy dissipated by the instabilities increases monotonically with n at each source setting, which means that not all instability events dissipate the same energy but rather that there is a correlation between the dissipated energy and the number of bursts associated with each event. It is worth noting that the RF power or neutral gas pressure has only a small effect on the energy dissipated by the instabilities, whereas the emitted energy per instability event increases strongly with the magnetic field strength. At a B_{min}/B_{ecr} of 0.83, the $n = 1$ mode dissipates more energy than any of the higher n modes (up to $n = 8$ detected) with a B_{min}/B_{ecr} of 0.76. This observation fortifies the notion that the magnetic field strength is the most influential ECRIS parameter in terms of the instabilities.

Figure 10 shows a representative plot with the average recovery and accumulation times vs the average energy released in each instability event for different n. An example of the scatter plots from which the average energy and the average recovery and accumulation times are calculated is presented in the supplementary material (Fig. S4). Figure 10 reveals that the recovery time following each instability event increases with n, the dependence being weak though while the accumulation time is practically independent on n. The independence of the accumulation time on the released energy has

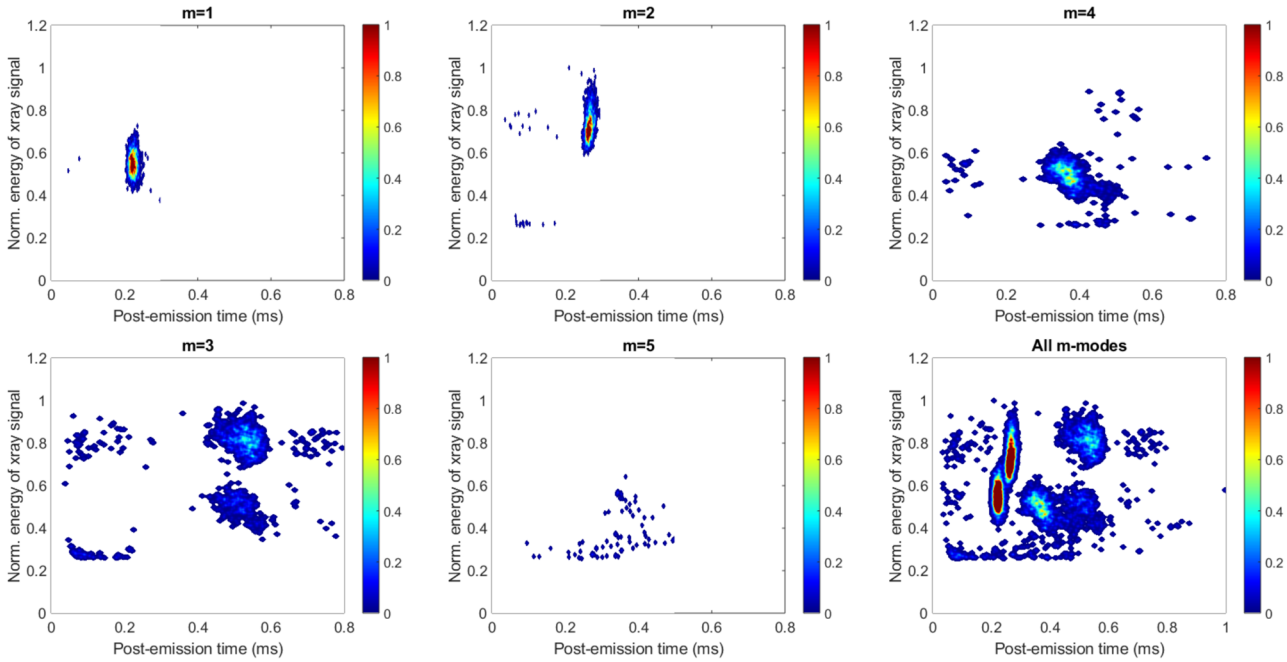

FIG. 13. The dependence of post-emission time on the energy emitted per burst mode m. The data corresponds to a B_{min}/B_{ecr} value of 0.76, neutral gas pressure of 3.5×10^{-7} mbar, and RF power of 400 W. The x-ray energy is normalized to the maximum value corresponding to all burst modes m combined. The plot shows individually each mode $m = 1, \ldots, 5$ and a combined plot of all m-modes. The false color represents the data point density, with blue representing the lowest.

been reported earlier in the context of magnetospheric plasmas, namely, the formation of pulsating auroras,[29] i.e., it seems to be a natural property of oscillatory regimes with low duty cycles, for which the energy release occurs in a much faster time scale than the accumulation of the energy.

Since the energy dissipated in each instability event increases monotonically with n, this implies that the time between instability events depends on their magnitude, a large amplitude emission leading to a longer recovery time until the next event, i.e., scenario (a) presented in the introduction is more likely than scenario (b). Our observation is similar to that made for magnetospheric plasmas where large amplitude quasi-periodic emissions lead to a long recovery time at high duty cycle regimes, i.e., when the on and off periods of the instabilities are nearly equal.[29,56] It is worth noting that at low duty cycles with randomly spaced instability bursts, the opposite, i.e., our scenario (b), was found for the magnetospheric plasma. The relevance of the recovery time over the accumulation time in our experiment is further highlighted in Fig. 11, showing an example of the (normalized) energy per event as a function of these characteristic times calculated from the scatter plots summing all event modes $n = 1, \ldots, 10$. There is a clear correlation between the released energy per event and the recovery time, whereas the accumulation time does not show much dependence on the released energy.

C. The effect of ion source parameters on the instability recovery time

After establishing that the time between instability events (recovery time) depends on the total energy of an instability event, i.e., a larger amplitude event leading to a longer recovery time until the next one, we studied the dependence of the instability recovery time on the ion source settings. The results are shown in Fig. 12. It was observed that the recovery time decreases with increasing $B_{\min}/B_{ecr}$ and microwave power, while varying the neutral gas pressure shows no prominent effect. This observation is attributed to the decrease in the instability event period (see Fig. 8), which is dominated by the recovery time. The recovery time itself is affected by the electron heating properties, namely, the magnetic field gradient and electric field strength. At the same time, the increased rate of inelastic collisions damping the cold and warm electron energy (<10 keV order of magnitude) at higher gas density has an insignificant effect on the development of the EED toward the instability threshold. This is attributed to the fact that the instabilities are driven by the high energy electrons for which the inelastic collision cross section is small.

D. Preliminary burst mode *m* analysis

In order to illustrate the temporal distribution of the m-mode bursts at a sub-millisecond time scale (within each n-mode event), a new parameter, *post-emission time,* is defined as shown in Fig. 6. It is defined as the time between two emission bursts (m) within an event (n) i.e., the post-emission time corresponding to burst $m = i$ is the time difference between bursts $m = i$ and $m = i + 1$. Figure 13 shows an example of the m-mode analysis, where the dependence of the post-emission time on the energy emitted per burst is presented as heat maps for $m = 1, \ldots, 5$. It is seen that the burst m emissions populate discrete regions when the (normalized) energy of the x-ray signal is plotted as a function of the post-emission time. This suggests that close to the instability threshold, the plasma self-organizes to release the excess energy, restoring stable conditions in a deterministic way, with quasi-periodic microwave and particle bursts.

When the rate of change of the plasma energy content and anisotropy (electron heating) is increased by making the $B_{\min}/B_{ecr}$ ratio higher and the average field gradient on the resonance surface lower, the quantized behavior becomes less evident. This is demonstrated in Fig. 14, showing the heat map distribution of bursts m in x-ray energy vs post-emission time phase space for two $B_{\min}/B_{ecr}$ values. In the case of higher $B_{\min}$, the x-ray emissions occupy a wider range of energies, yet most of them are found at the same level as with the lower $B_{\min}$. At the same time, the distribution of post-emission times approaches a continuum. On the other hand, as shown in Fig. 15, the average event time increases almost linearly

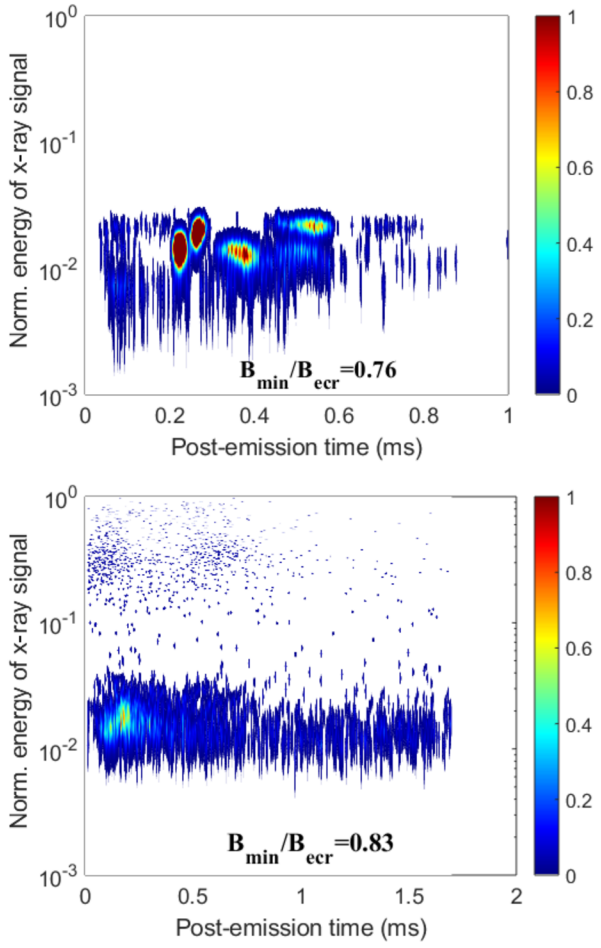

FIG. 14. The dependence of the post-emission time on the energy emitted per burst m. The data corresponds to a $B_{\min}/B_{ecr}$ value 0.76 and 0.83, neutral gas pressure of 3.5×10^{-7} mbar, and RF power of 400 W. The x-ray energy range on the vertical axes is normalized to the maximum value corresponding to the higher $B_{\min}/B_{ecr}$ value.

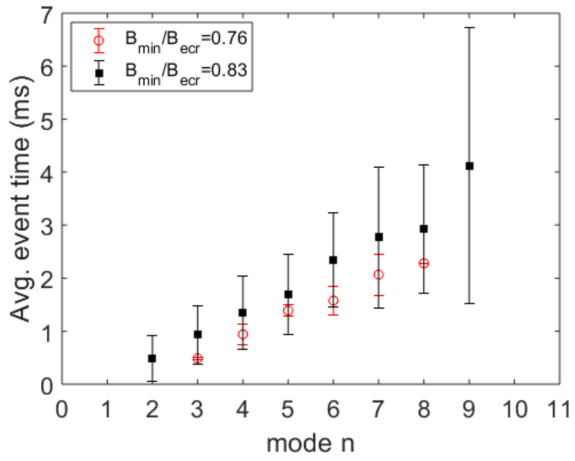

FIG. 15. The event time as a function of n for two different B_{min}/B_{ecr} values with 400 W RF power and 3.5×10^{-7} mbar neutral gas pressure.

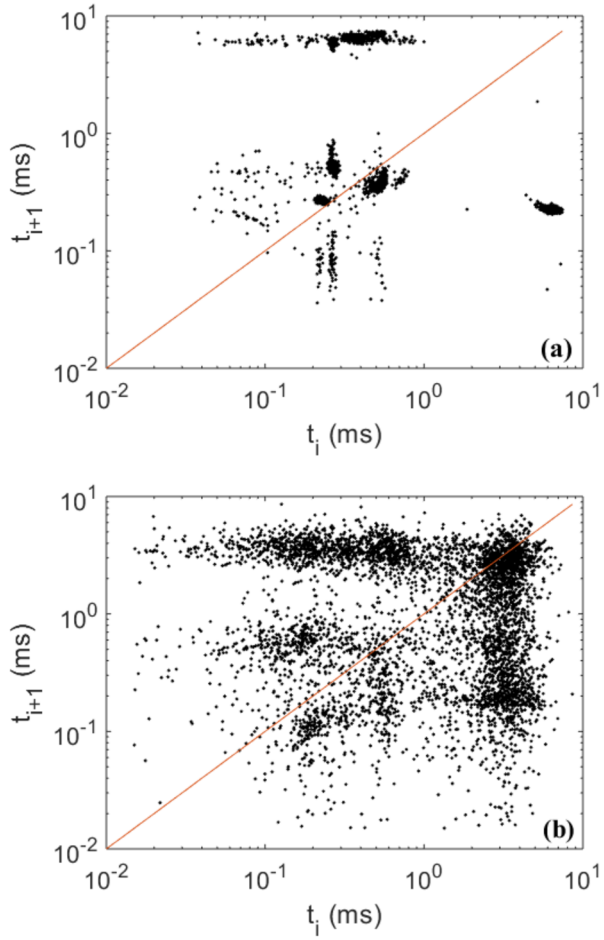

FIG. 16. Poincaré maps showing the time difference between a particular emission burst i and the following burst $i + 1$. (a) B_{min}/B_{ecr} of 0.76 and (b) B_{min}/B_{ecr} of 0.83. The neutral gas pressure is 3.5×10^{-7} mbar and the RF power is 400 W in both cases.

with n but is not strongly affected by the field strength, whereas its standard deviation becomes larger at high B_{min}. This follows from the fact that the instability bursts within each event become more sporadic as the plasma energy content and anisotropy of the EED increase.

In qualitative terms, the data in Fig. 14 can be interpreted as a transition of the non-linear system (quasi-periodic maser-type cyclotron instability) from an organized chaotic system to an unorganized one with the increase of the energy content and anisotropy of the EED. This behavior is analogous to the famous dripping faucet experiment;[57,58] the expulsion of energy from the plasma can be compared to the behavior of the droplet formation interval. The development of chaos is well described by a Poincaré map, which consists of plotting the time lapse before vs after the occurrence of several consecutive instability events.

The Poincaré maps shown in Fig. 16 represent the data collected at B_{min}/B_{ecr} values of 0.76 and 0.83. The plots compile all successive instability bursts measured during the 10 s data acquisition, i.e., neither n or m mode dichotomy is considered. At a B_{min}/B_{ecr} of 0.76 the Poincaré map consists of separate regions populated by data points. Increasing the B_{min} results in a (semi-)continuous distribution of instability bursts in the time domain, which, following the literature,[57,58] is interpreted as a transition toward a more chaotic instability regime, where the energy release and its periodicity become erratic.

V. CONCLUSION

In this paper, we have presented the main findings of a phenomenological investigation of the occurrence of cyclotron maser instabilities in a minimum-B magnetic device (ECR ion source). These can be summarized as follows:

- The quasi-periodic plasma instabilities are often grouped into bursts of microwaves and electrons from the magnetic confinement. Such grouping has been observed previously in a minimum-B ECRIS as a by-product of experiments focusing on the suppression of the instabilities,[22] but it has not been discussed at all in the literature. The occurrence of grouped instability bursts implies that there is a fundamental limit of the energy dissipated by a single burst, i.e., the release of the stored energy carried by the hot tail of the EED requires several instability onsets within an event. The physical reason for the grouping in the minimum-B trap is not currently understood. It is worth noting that the oscillatory behavior of the cyclotron instability with clearly distinguishable on and off phases is a key mechanism applied for explaining quasi-periodic low frequency emissions and related auroral pulsations in magnetospheric plasmas.[59,60] The relation between the characteristic times of the oscillating instability regimes has been considered for these natural phenomena both theoretically and experimentally.[29,56] Our work demonstrates that controllable minimum-B laboratory plasmas could be used as a proxy for naturally occurring large-scale plasmas and invites further theoretical studies to explain the observations.
- The instability event period and recovery time decrease with an increase in B_{min}/B_{ecr} ratio and RF power and not with

pressure, which can be attributed to the increase in plasma energy density.[61]

- The quiescent time between instability events depends on the energy dissipated by the instabilities, i.e., a sequence of bursts dissipating a larger amount of energy leads to a longer recovery time until the next event than the bursts dissipating less energy. In other words, there is a correlation between the instability recovery time and the dissipated energy, whereas there is no correlation between the instability accumulation time and the dissipated energy. We explain this (qualitatively) as follows: Instabilities dissipating a large amount of energy restore a stable EED with a lower energy content than small amplitude instabilities. The energy content of the EED is then accumulating at the rate defined by the electron heating affected by magnetic field and microwave power (indicated by the decreasing instability event period/increasing repetition rate with these parameters shown in Fig. 8) until the instability threshold level of EED anisotropy is reached again.
- Plasma energy losses associated with each instability burst appear to be self-organized near the instability threshold (at low $B_{\min}/B_{ecr}$ and RF power), i.e., the bursts are periodic and are associated with quantized energy (particle) losses. However, as the energy content of the plasma increases with the magnetic field strength, the energy release associated with the instability shifts from deterministic to chaotic with trains of randomly spaced (in time) energy and particle bursts of varying amplitude.

We invite the plasma theory community to explain our experimental findings, especially the grouping of events and discrete timing of the instability bursts within the events.

SUPPLEMENTARY MATERIAL

See the supplementary material for additional details of the instability signal treatment, data analysis, selection of diagnostic signals for analysis, and reproducibility of the results.

ACKNOWLEDGMENTS

We would like to thank Ivan Izotov and Vadim Skalyga of the IAP-RAS for fruitful discussions regarding the experiment. We would also like to thank Risto Kronholm of JYFL for providing the necessary technical assistance. This work was supported by the Academy of Finland Project funding (Grant No. 315855) and the University of Grenoble Alpes under the EMERGENCE program.

AUTHOR DECLARATIONS

Conflict of Interest

The authors have no conflicts to disclose.

DATA AVAILABILITY

The data that support the findings of this study are available from the corresponding author upon reasonable request.

REFERENCES

[1] A. G. Shalashov, E. D. Gospodchikov, I. V. Izotov, D. A. Mansfeld, V. A. Skalyga, and O. Tarvainen, "Control of electron-cyclotron instability driven driven by strong ECRH in open magnetic trap," Europhys. Lett. **124**(3), 35001 (2018).
[2] B. Eliasson, M. Viktorov, D. C. Speirs, K. Ronald, D. Mansfeld, and A. D. R. Phelps, "Observation of electron cyclotron harmonic emissions due to electrostatic instabilities in mirror-confined plasma," Phys. Rev. Res. **2**, 043272 (2020).
[3] R. C. Garner, M. E. Mauel, S. A. Hokin, R. S. Post, and D. L. Smatlak, "Warm electron driven whistler instability in an electron-cyclotron-resonance heated, mirror-confined plasma," Phys. Rev. Lett. **59**(16), 1821–1824 (1987).
[4] A. Vodopyanov, S. Golubev, A. Demekhov, V. Zorin, D. Mansfeld, S. Razin, and V. Trakhtengerts, "Laboratory modeling of nonstationary processes in space cyclotron masers: First results and prospects," Plasma Phys. Rep. **31**(11), 927–937 (2005).
[5] I. Izotov, O. Tarvainen, D. Mansfeld, V. Skalyga, H. Koivisto, T. Kalvas, J. Komppula, R. Kronholm, and J. Laulainen, "Microwave emission related to cyclotron instabilities in a minimum-B electron cyclotron resonance ion source plasma," Plasma Sources Sci. Technol. **24**(4), 045017 (2015).
[6] I. Izotov, T. Kalvas, H. Koivisto, R. Kronholm, D. Mansfeld, V. Skalyga, and O. Tarvainen, "Broadband microwave emission spectrum associated with kinetic instabilities in minimum-B ECR plasmas," Phys. Plasmas **24**(4), 043515 (2017).
[7] I. Izotov, O. Tarvainen, V. Skalyga, D. Mansfeld, H. Koivisto, R. Kronholm, V. Toivanen, and V. Mironov, "Measurements of the energy distribution of electrons lost from the minimum B-field-the effect of instabilities and two-frequency heating," Rev. Sci. Instrum. **91**(1), 013502 (2020).
[8] O. Tarvainen, I. Izotov, D. Mansfeld, V. Skalyga, S. Golubev, T. Kalvas, H. Koivisto, J. Komppula, R. Kronholm, J. Laulainen, and V. Toivanen, "Beam current oscillations driven by cyclotron instabilities in a minimum-B electron cyclotron resonance ion source plasma," Plasma Sources Sci. Technol. **23**(2), 025020 (2014).
[9] O. Tarvainen, R. Kronholm, T. Kalvas, H. Koivisto, I. Izotov, V. Skalyga, V. Toivanen, and L. Maunoury, "The biased disc of an electron cyclotron resonance ion source as a probe of instability-induced electron and ion losses," Rev. Sci. Instrum. **90**(12), 123303 (2019).
[10] O. Tarvainen, J. Laulainen, J. Komppula, R. Kronholm, T. Kalvas, H. Koivisto, I. Izotov, D. Mansfeld, and V. Skalyga, "Limitations of electron cyclotron resonance ion source performances set by kinetic plasma instabilities," Rev. Sci. Instrum. **86**(2), 023301 (2015).
[11] O. Tarvainen, T. Kalvas, H. Koivisto, J. Komppula, R. Kronholm, J. Laulainen, I. Izotov, D. Mansfeld, V. Skalyga, V. Toivanen, and G. Machicoane, "Limitation of the ECRIS performance by kinetic plasma instabilities," Rev. Sci. Instrum. **87**(2), 02A703 (2016).
[12] S. V. Golubev and A. G. Shalashov, "Cyclotron-resonance maser driven by magnetic compression of rarefied plasma," Phys. Rev. Lett. **99**(20), 205002 (2007).
[13] I. V. Izotov, A. G. Shalashov, V. A. Skalyga, E. D. Gospodchikov, O. Tarvainen, V. E. Mironov, H. Koivisto, R. Kronholm, V. Toivanen, and B. Bhaskar, "The role of radio frequency scattering in high-energy electron losses from minimum-B ECR ion source," Plasma Phys. Controlled Fusion **63**(4), 045007 (2021).
[14] J. Benitez, C. Lyneis, L. Phair, D. Todd, and D. Xie, "Dependence of the bremsstrahlung spectral temperature in minimum-B electron cyclotron resonance ion sources," IEEE Trans. Plasma Sci. **45**(7), 1746–1754 (2017).
[15] B. S. Bhaskar, H. Koivisto, O. Tarvainen, T. Thuillier, V. Toivanen, T. Kalvas, I. Izotov, V. Skalyga, R. Kronholm, and M. Marttinen, "Correlation of bremsstrahlung and energy distribution of escaping electrons to study the dynamics of magnetically confined plasma," Plasma Phys. Controlled Fusion **63**(9), 095010 (2021).
[16] E. Naselli, D. Mascali, M. Mazzaglia, S. Biri, R. Rácz, J. Pálinkás, Z. Perduk, A. Galatá, G. Castro, L. Celona, S. Gammino, and G. Torrisi, "Impact of two-close-frequency heating on ECR ion source plasma radio emission and stability," Plasma Sources Sci. Technol. **28**(8), 085021 (2019).
[17] B. Isherwood, "Characterization of electron cyclotron resonance ion source instabilities by charged particle diagnostics," Ph.D. thesis, Michigan State University, 2020, https://pa.msu.edu/sites/_pa/assets/File/Isherwood_Thesis.pdf.

[18]V. A. Skalyga, I. V. Izotov, A. G. Shalashov, E. D. Gospodchikov, E. M. Kiseleva, O. Tarvainen *et al.*, "Controlled turbulence regime of electron cyclotron resonance ion source for improved multicharged ion performance," J. Phys. D: Appl. Phys. **54**(38), 385201 (2021).
[19]A. G. Shalashov, E. D. Gospodchikov, I. V. Izotov, D. A. Mansfeld, V. A. Skalyga, and O. Tarvainen, "Observation of Poincaré-Andronov-Hopf bifurcation in cyclotron maser emission from a magnetic plasma trap," Phys. Rev. Lett. **120**, 1555001 (2018).
[20]A. G. Shalashov, S. V. Golubev, E. D. Gospodchikov, D. A. Mansfeld, and M. E. Viktorov, "Interpretation of complex patterns observed in the electron-cyclotron instability of a mirror confined plasma produced by an ECR discharge," Plasma Phys. Controlled Fusion **54**(8), 085023 (2012).
[21]A. G. Shalashov, E. D. Gospodchikov, and I. V. Izotov, "Electron-cyclotron heating and kinetic instabilities of a mirror-confined plasma: The quasilinear theory revised," Plasma Phys. Controlled Fusion **62**(6), 065005 (2020).
[22]V. Skalyga, I. Izotov, T. Kalvas, H. Koivisto, J. Komppula, R. Kronholm, J. Laulainen, D. Mansfeld, and O. Tarvainen, "Suppression of cyclotron instability in electron cyclotron resonance ion sources by two-frequency heating," Phys. Plasmas **22**, 083509 (2015).
[23]S. V. Golubev and A. G. Shalashov, "Cyclotron-resonance maser with adiabatic magnetic pumping in a low-density plasma," JETP Lett. **86**(2), 91–97 (2007).
[24]V. Trakhtengerts and M. Rycroft, *Whistler and Alfven Mode Cyclotron Masers in Space* (Cambridge University Press, 2008).
[25]V. Ginzburg, *The Propagation of Electromagnetic Waves in Plasmas* (Pergamon, Oxford, 1970).
[26]A. G. Demekhov, "Cyclotron instability of the slow extraordinary wave in a magnetoactive plasma," Radiophys. Quantum Electron. **30**, 547–557 (1987).
[27]A. V. Vodopyanov, S. V. Golubev, A. G. Demekhov, V. G. Zorin, D. A. Mansfeld, S. V. Razin, and A. G. Shalashov, "Observation of pulsed fast electron precipitations and the cyclotron generation mechanism of burst activity in a decaying ECR discharge plasma," J. Exp. Theor. Phys. **104**, 296–306 (2007).
[28]B. Isherwood, G. Machicoane, D. Neben, G. Pozdeyev, and J. Stetson, "Plasma instability studies of the SuSI 18 GHz source," in *Proceedings of the 23rd International Workshop on ECR Ion Sources (ECRIS'18), International Workshop on ECR Ion Sources*, Catania, Italy, 10–14 September 2018, http://www.jacow.org, pp. 157–161.
[29]A. G. Demekhov and V. Y. Trakhtengerts, "A mechanism of formation of pulsating aurorae," J. Geophys. Res. **99**(4), 5831–5841, https://doi.org/10.1029/93ja01804 (1994).
[30]E. A. Benediktov, G. G. Getmantsev, N. A. Mityakov, V. O. Rapoport, and A. F. Tarasov, "On relationship of sporadic radio emission registered on satellites of the 'Elektron' series with the geomagnetic activity," Cosmic Res. **6**, 791 (1968), https://ntrs.nasa.gov/citations/19690006158.
[31]D. Grunett, "Electromagnetic plasma wave emissions from the auroral field lines," J. Geomagn. Geoelectr. **30**(3), 257–272 (1978).
[32]C. Trigilio, P. Leto, G. Umana, C. S. Buemi, and F. Leone, "Auroral radio emission from stars: The case of CU virginis," Astrophys. J., Lett. **739**(1), L10 (2011).
[33]H. Koivisto, P. Heikkinen, V. Hänninen, A. Lassila, H. Leinonen, V. Nieminen, J. Pakarinen, K. Ranttila, J. Ärje, and E. Liukkonen, "The first results with the new JYFL 14 GHz ECR ion source," Nucl. Instrum. Methods Phys. Res., Sect. B **174**(3), 379–384 (2001).
[34]O. Tarvainen, T. Lamy, J. Angot, T. Thuillier, P. Delahaye, L. Maunoury, J. Choinski, L. Standylo, A. Galatà, G. Patti, and H. Koivisto, "Injected 1+ ion beam as a diagnostics tool of charge breeder ECR ion source plasmas," Plasma Sources Sci. Technol. **24**, 035014 (2015).
[35]V. Mironov, S. Bogomolov, A. Bondarchenko, A. Efremov, V. Loginov, and D. Pugachev, "Spatial distributions of plasma potential and density in electron cyclotron resonance ion source," Plasma Sources Sci. Technol. **29**, 065010 (2020).
[36]D. Mascali, L. Neri, L. Celona, G. Castro, G. Torrisi, S. Gammino, G. Sorbello, and G. Ciavola, "A double-layer based model of ion confinement in electron cyclotron resonance ion source," Rev. Sci. Instrum. **85**, 02A511 (2014).
[37]C. Barué, M. Lamoureux, P. Briand, A. Girard, and G. Melin, "Investigation of hot electrons in electron-cyclotron-resonance ion sources," J. Appl. Phys. **76**, 2662 (1994).
[38]G. Douysset, H. Khodja, A. Girard, and J. P. Briand, "Highly charged ion densities and ion confinement properties in an electron-cyclotron-resonance ion source," Phys. Rev. E **61**(3), 3015–2022 (2000).
[39]V. Toivanen, B. S. Bhaskar, I. V. Izotov, H. Koivisto, and O. Tarvainen, "Diagnostic techniques of minimum-B ECR ion source plasma instabilities," Rev. Sci. Instrum. **93**(1), 013302 (2022).
[40]See https://www.thinksrs.com/products/sr570.html for Stanford Research Systems preamplifier.
[41]See https://www.picotech.com/oscilloscope/5000/flexible-resolution-oscilloscope for Picoscope 5000 series.
[42]O. Tarvainen, T. Kalvas, H. Koivisto, J. Komppula, R. Kronholm, J. Laulainen, I. Izotov, D. Mansfeld, and V. Skalyga, "Kinetic instabilities in pulsed operation mode of a 14 GHz electron cyclotron resonance ion source," Rev. Sci. Instrum. **87**, 02A701 (2016).
[43]I. Izotov, D. Mansfeld, V. Skalyga, V. Zorin, T. Grahn, T. Kalvas, H. Koivisto, J. Komppula, P. Peura, O. Tarvainen, and V.Toivanen, "Plasma instability in the afterglow of electron cyclotron resonance discharge sustained in a mirror trap," Phys. Plasmas **19**, 122501 (2012).
[44]I. Izotov, T. Kalvas, H. Koivisto, J. Komppula, R. Kronholm, J. Laulainen, D. Mansfeld, V. Skalyga, and O. Tarvainen, "Cyclotron instability in the afterglow mode of minimum-B ECRIS," Rev. Sci. Instrum. **87**, 02A729 (2016).
[45]J. Orpana, O. Tarvainen, T. Kalvas, H. Koivisto, R. Kronholm, J. Laulainen, I. Izotov, D. Mansfeld, and V. Skalyga, "Measurement of microwave frequencies emitted by instabilities of ECRIS plasma with waveguide filters and microwave sensitive diodes," in *Proceedings of the 22nd International Workshop on ECR Ion Sources (ECRIS2016), International Workshop on ECR Ion Sources*, Busan, Korea, 28 August–1 September 2016, http://www.jacow.org, pp. 133–136.
[46]O. Tarvainen, J. Angot, I. Izotov, V. Skalyga, H. Koivisto, T. Thuillier, T. Kalvas, and T. Lamy, "Plasma instabilities of a charge breeder ECRIS," Plasma Sources Sci. Technol. **26**, 105002 (2017).
[47]O. Tarvainen, V. Toivanen, J. Komppula, T. Kalvas, and H. Koivisto, "Transverse distribution of beam current oscillations of a 14 GHz electron cyclotron resonance ion source," Rev. Sci. Instrum. **85**, 02A909 (2014).
[48]O. Tarvainen, J. Angot, I. Izotov, V. Skalyga, H. Koivisto, T. Thuillier, T. Kalvas, V. Toivanen, R. Kronholm, and L. Lamy, "The effect of plasma instabilities on the background impurities in charge breeder ECRIS," AIP Conf. Proc. **2011**, 070006 (2018).
[49]V. Toivanen, O. Tarvainen, J. Komppula, and H. Koivisto, "Oscillations of ECR ion source beam current along the beam transport of the JYFL K-130 cyclotron," J. Instrum. **8**(2), T02005 (2013).
[50]R. Kronholm, T. Kalvas, H. Koivisto, and O. Tarvainen, "Spectroscopic method to study low charge state ion and cold electron population in ECRIS plasma," Rev. Sci. Instrum. **89**(4), 043506 (2018).
[51]R. Kronholm, T. Kalvas, H. Koivisto, S. Kosonen, M. Marttinen, D. Neben, M. Sakildien, O. Tarvainen, and V. Toivanen, "ECRIS plasma spectroscopy with a high resolution spectrometer," Rev. Sci. Instrum. **91**(1), 013318 (2020).
[52]A. G. Demekhov and V. Y. Trakhtengerts, "Several questions on radiation dynamics in magnetic plasma traps," Radiophys. Quantum Electron. **29**, 848–857 (1986).
[53]S. Gammino, D. Mascali, L. Celona, F. Maimone, and G. Ciavola, "Considerations on the role of the magnetic field gradient in ECR ion sources and build-up of hot electron component," Plasma Sources Sci. Technol. **18**(4), 045016 (2009).
[54]J. B. Li, L. X. Li, B. S. Bhaskar, V. Toivanen, O. Tarvainen, D. Hitz, L. B. Li, W. Lu, H. Koivisto, T. Thuillier, J. W. Guo, X. Z. Zhang, H. Y. Zhao, L. T. Sun, and H. W. Zhao, "Effects of magnetic configuration on hot electrons in a minimum-B ECR plasma," Plasma Phys. Controlled Fusion **62**(9), 095015 (2020).
[55]M. C. Williamson, A. J. Lichtenberg, and M. A. Lieberman, "Self-consistent electron cyclotron resonance absorption in a plasma with varying parameters," J. Appl. Phys. **72**(9), 3924–3933 (1992).

[56]D. L. Pasmanik, A. G. Demekhov, M. Hayoš, F. NĚmec, O. Santolík, and M. Parrot, "Quasiperiodic ELF/VLF emissions detected onboard the DEMETER spacecraft: Theoretical analysis and comparison with observations," J. Geophys. Res.: Space Phys. **124**(7), 5278–5288, https://doi.org/10.1029/2018ja026444 (2019).
[57]P. Martien, S. C. Pope, P. L. Scott, and R. S. Shaw, "The chaotic behavior of the leaky faucet," Phys. Lett. A **110**(7–8), 399–404 (1985).
[58]R. F. Cahalan, H. Leidecker, and G. D. Cahalan, "Chaotic rhythms of a dripping faucet: A simple drop detector transforms the computer into a temporal microscope, revealing a variety of rhythms in the common leaky tap," Comput. Phys. **4**(4), 368–382 (1990).
[59]G. T. Davidson and Y. T. Chiu, "A closed nonlinear model of wave-particle interactions in the outer trapping and morningside auroral regions," J. Geophys. Res.: Space Phys. **91**(A12), 13705–13710, https://doi.org/10.1029/ja091ia12p13705 (1986).
[60]V. Yu. Trakhtengerts, V. R. Tagirov, and S. A. Chernouss, "A circulating cyclotron maser and pulsed VLF emissions," Geomagn. Aeron. **26**(1), 77–82 (1986).
[61]J. Noland, "Measurements of plasma bremsstrahlung and plasma energy density produced by electron cyclotron resonance ion source plasmas," Ph.D. thesis, University of California, Berkeley, 2011, https://digitalassets.lib.berkeley.edu/etd/ucb/text/Noland_berkeley_0028E_11247.pdf.